Acta Cryst. (1997). D**53**, 143–150

Structure of Diisopropyl Fluorophosphate-Inhibited Factor D

L. Brent Cole,[a]* Naiming Chu,[a] J. Michael Kilpatrick,[a] John E. Volanakis,[b] S. V. L. Narayana[c] and Y. Sudhakar Babu[a]

[a]*BioCryst Pharmaceuticals, Inc., 2190 Parkway Lake Drive, Birmingham, AL 35244-2812, USA,* [b]*Division of Clinical Immunology and Rheumatology, University of Alabama at Birmingham, Birmingham, AL 35294, USA, and* [c]*Center for Macromolecular Crystallography, University of Alabama at Birmingham, Birmingham, AL 35294, USA. E-mail: cole@orion.cmc.uab.edu*

(*Received 13 June 1996; accepted 17 October 1996*)

Abstract

Factor D (D) is a serine protease, crucial for the activation of the alternative complement pathway. Only a limited number of general serine protease inhibitors are known to inhibit D, most of which covalently bind to the serine hydroxyl of the catalytic triad. The structure of the first enzyme:inhibitor covalent adduct of D with diisopropyl fluorophosphate (DIP:D) to a resolution of 2.4 Å is described. The inhibited enzyme is similar in overall structure to the native enzyme and to trypsin, yet exhibits notable differences in the active site. One region of the active site is conserved between D and trypsin with respect to amino-acid sequence and to conformation. Another reflects the amino-acid substitutions and conformational flexibility between these enzymes. The active-site histidine residue is observed in the *gauche*+ conformation, not the normal *gauche*− orientation seen in the classic catalytic triad arrangement required for enzymatic activity in serine proteases. Comparisons of the active sites between native D, the DIP:D adduct, and DIP-inhibited trypsin have provided fundamental insights currently being employed in the design of novel small-molecule pharmaceutical agents capable of modulating the alternative complement pathway.

1. Introduction

Factor D (D) is an integral serum serine protease required for the formation of C3 convertase in the alternative pathway of complement activation. D has only one known natural substrate, cleaving a single Arg233—Lys234 bond of factor B (B), when B is in the Mg^{2+}-dependent complex C3bB (Lesavre, Hugli, Esser & Muller-Eberhard, 1979). The enzyme is tightly regulated, circulating at the lowest concentration of all complement proteins, $1.8 \pm 0.4\ \mu g\ ml^{-1}$ (Barnum, Niemann, Kearney & Volanakis, 1984), with highly restrictive substrate specificity. No zymogen form of the enzyme exists in the blood (Lesavre & Muller-Eberhard, 1978). In fact, D is the limiting enzyme in the cascading sequence of the alternative pathway (Lesavre & Muller-Eberhard, 1978). Although complement is one of the key effector mechanisms of host defense responding to infection or injury, inappropriate activation of complement can cause medical complications. Complement activation is believed to be involved in the inflammatory reactions which accompany myocardial infarction (heart attack), adult respiratory distress syndrome (ARDS), and post-heart-attack reperfusion injury (Yasuda *et al.*, 1990; Hansson, Jonasson, Seifert & Stemme, 1989; Cryer, Richardson, Longmire-Cook & Brown, 1989). Since it is the limiting enzyme in the alternative complement pathway, and is positioned early in the cascade, D is the logical choice for pharmacological control of complement activation.

D is a single polypeptide chain, $M_r = 24$ kDa, exhibiting a high degree of amino-acid sequence identity with other serine proteases, in particular, pancreatic bovine trypsin, chymotrypsin A, human neutrophil elastase, porcine elastase, and rat mast-cell protease (Niemann, Brown, Bennett & Volanakis, 1984). In comparison with other members of the serine protease superfamily, D has very low catalytic activity against synthetic ester substrates (Kam *et al.*, 1987), reacts moderately with isocoumarin inhibitors of serine proteases (Kam, Oglesby, Pangburn, Volanakis & Powers, 1992), and can be completely inactivated by diisopropyl fluorophosphate (DFP) (Fearon, Austen & Ruddy, 1974), the focus of this paper.

D circulates in the blood as a potentially active protein, not as a zymogen, yet is devoid of proteolytic activity against uncomplexed B. Thus, it has been postulated that a conformational change is induced in B upon its binding to C3b (Lesavre & Muller-Eberhard, 1978). As a result of the low catalytic activity of the enzyme toward thioester substrates, it has also been suggested that a conformational change in the active site of D may be induced by its substrate, the C3bB complex (Kam *et al.*, 1987). The structure of native D has been solved to 2.0 Å resolution (Narayana *et al.*, 1994), demonstrating that the protein exhibits the same general structural fold as the serine protease superfamily, yet the catalytic triad residues are not positioned in a manner conducive to efficient catalysis. The examina-

tion of key amino-acid sequence differences compared with other serine proteases, the conformational differences in the loops of the active site, and substrate specificity pockets of the enzyme, provides some insight into the 'zymogen-like' conformation of the native enzyme. In light of its pivotal role in complement activation, the techniques of structure-based drug design (reviewed by Bugg, Carson & Montgomery, 1993) are currently being applied in the design of novel small-molecule inhibitors of D. To gain insight into the specificity and function of the active site of this unique serine protease, we crystallized the enzyme which had been completely inactivated by covalent modification with DFP. Here, we report the structure of the enzyme:inhibitor adduct, DIP:D, to 2.4 Å resolution.

Table 1. *Intensity data collection and refinement statistics for DIP:D*

Resolution (Å)	2.4
Number of crystals	2
Number of observations	64 840
Number of unique reflections	14 663
Completeness (%)	95.4
Merging *XENGEN R* factor (%)	8.2
Number of reflections used in *X-PLOR* refinement (8–2.4 Å, $I > 2\sigma$) of the dimer	13 754
Number of protein atoms	3424
Number of inhibitor atoms	20
Number of water molecules	262
R factor	0.151
R.m.s. deviation from ideal bond lengths (Å)	0.010
R.m.s. deviation from ideal bond angles (°)	1.7
R.m.s. deviation from ideal dihedral angles (°)	27.1
R.m.s. deviation from ideal improper dihedral angles (°)	1.4

2. Experimental

2.1. *Crystallization*

Freshly isolated D (Volanakis & Macon, 1987) was dialyzed exhaustively against 10 m*M* Tris buffer, pH = 7.0, 100 m*M* NaCl, then concentrated to 8 mg ml^{-1}. To 99 µl of this protein solution, 1 µl of a 1.0 *M* DFP (in isopropanol) solution was added, yielding a final concentration of 10 m*M* DFP. The solution was allowed to incubate for 24 h at 277 K before crystallization trials were set up. Hemolytic assays (Volanakis, Barnum & Kilpatrick, 1993) were conducted using the DFP-treated D, confirming 99% inhibition of the protein. Small block-shaped crystals were produced by hanging-drop vapor diffusion against a well solution of 50 m*M* MES, pH = 5.6–5.8, 12–16% polyethylene glycol 6000, 0.2 *M* NaCl. Diffraction-quality crystals were then obtained using a macroseeding technique similar to that described by Thaller *et al.* (1981). The largest crystals were grown using macroseeded sitting drops under the conditions above, with the exception of a beginning drop ratio of 2:1 µl protein to reservoir solution.

2.2. *Data collection*

The enzyme crystallized in space group $P2_1$, with unit-cell dimensions $a = 40.6$, $b = 125.7$, $c = 41.9$ Å, $\beta = 110.5°$. The asymmetric unit consists of a dimer, which exhibits approximate twofold non-crystallographic symmetry (177.6° rotation). Intensity data to 2.4 Å were collected on a Siemens multiwire area detector mounted on a Rigaku RU-200 rotating-anode X-ray generator and processed using the *XENGEN* suite of programs (Howard *et al.*, 1987). Relevant data-collection statistics are recorded in Table 1.

2.3. *Structure refinement*

Initial phases were obtained by the method of molecular replacement as implemented in *X-PLOR* (Brünger, 1990, 1992*a*). The search model was based upon the atomic coordinates of one monomer of the native D structure (Narayana *et al.*, 1994). Initially, intensity data for 15.0–4.0 Å collected from one crystal were used in the rotation and translation searches. Correct placement of the two monomers, labelled DIPA and DIPB, in the unit cell was straightforward. The two top peaks from the rotation search were 4.56σ and 4.05σ above the mean, respectively, with the next highest peak at 3.7σ. The rotated monomers were then translated into the unit cell separately, followed by a final translation search solution for the oriented dimer (11.9σ above the mean), resulting in a conventional crystallographic *R* factor of 0.436. Subsequent rigid-body refinement in *X-PLOR*, treating the monomers as individual rigid bodies, lowered the *R* factor to 0.389 for 15.0–4.0 Å data. Following one cycle of energy minimization in *X-PLOR* (*R* factor dropped to 0.268 for 6.0–2.5 Å data), electron-density maps were generated from calculated phases based on the roughly refined model using the Fourier coefficients $2F_{obs} - F_{calc}$ and $F_{obs} - F_{calc}$; these revealed good density for the majority of the protein of both monomers and clear density extending from the hydroxyl O atom of the active-site serine residues. Additional data were collected, processed and merged to yield the final data set represented in Table 1.

Iterative cycles of simulated annealing with molecular dynamics using *X-PLOR* followed by model rebuilding using the program *FRODO* (Jones, 1978) were conducted. Early attempts were made to utilize non-crystallographic restraints to refine the two monomers as one, but the *R* factors for such refinements increased significantly and the corresponding electron-density maps were noticeably of poorer quality in regions of intermolecular contacts. Three loop regions in each monomer exhibited broken density (residues A59–A63, A93–A105, A214–A225, B59–B63, B93–B105, and B214–B225). The regions A93–A105, B93–B105 and B214–B225 improved gradually through the

use of $2F_{obs} - F_{calc}$ and $F_{obs} - F_{calc}$ omit maps. The loop region A214–A225 improved moderately, with broken density still observed from residues A214–A219. The highly solvent-exposed loop regions A59–A62 and B59–B62 remained disordered. This yielded a model with an R factor of 0.219. Refinement of the structure of the protein continued as the resolution range was extended to include 8.0–2.4 Å data. Addition of the DIP moieties and solvent molecules lowered the R factor to 0.184. After temperature-factor refinement, the structure of the enzyme:inhibitor adduct ultimately converged to an R factor of 0.151. The quality of the refinement of DIP:D enzyme has been evaluated by *PROCHECK* (Laskowski, MacArthur, Moss & Thornton, 1993). The Ramachandran plots (Figs. 1*a* and 1*b* for DIPA and DIPB, respectively) identify residues A61b and B61b to be in disallowed regions. These residues are again located in a disordered loop and cannot be built into density with confidence. Residues A172, B172 and B174 lie in borderline regions, yet all three clearly fit the electron-density map well. Main- and side-chain parameters are indicative of a well refined structure.

3. Results and discussion

3.1. *General structure of the enzyme:inhibitor adduct*

The DIP:D inhibited enzyme crystallized as a dimer, as does the native enzyme, although the enzyme is active as a monomer in the blood. The overall structure of each monomer generally resembles that of the native enzyme, as well as the broad class of serine proteases (Fig. 2). Both monomers display an ellipsoidal shape with two domains, consisting primarily of twisted β-sheet structure, concluding in a C-terminal helix. The active-site region, containing the catalytic triad residues Asp102, His57 and Ser195, lies in the juncture between two β-sheet domains. (The chymotrysin numbering system is used for these serine proteases, accounting for insertions and deletions. Residues in the monomers DIPA and DIPB are numbered from A16 to A245 and from B16 to B245, as is the native enzyme. Residues from individual molecules will be cited only when major differences between the two monomers exists.) The four disulfide bridges, between the half-cystine residues 42 and 58, 136 and 201, 168 and 182, and 193 and 220, remains consistent with those of the native enzyme. These bridges tightly hold conserved-loop regions in place.

As a dimer, the two monomer active sites face opposite each other, related by an approximate non-crystallographic twofold axis (Fig. 3). The principal contacts across the twofold axis begin with a type-I turn (residues 118–121), continuing as a long stretch of β-strand (residues 121–131) along with another β-turn (residues 201–208) which extends toward the other monomer. Unlike the native enzyme, ordered solvent molecules have been located between the two monomers.

The superposition of the two monomers shows the two molecules to be very similar in the overall shape of the molecule, with only minor variations in the side-chain conformations. The 'left-hand' side of the active site, residues 215–220, appears to be more disordered, possibly because of greater conformational flexibility than the 'right-hand' side, residues 189–195. The electron density for the entire active site in the DIPB monomer is very clear for both the main chain and the

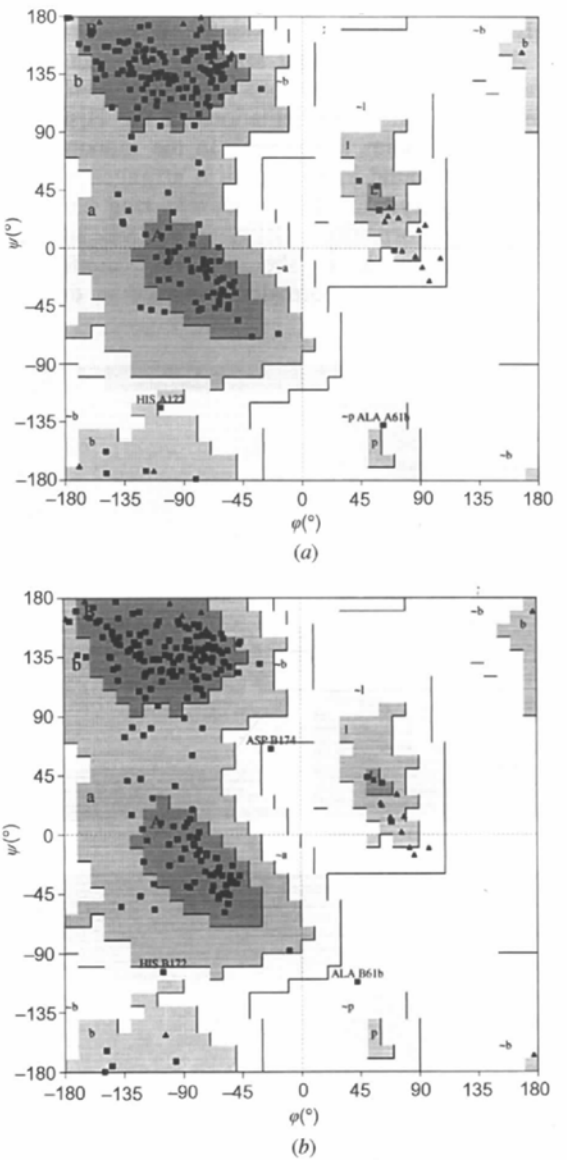

Fig. 1. (*a*) Ramachandran plot for the main-chain torsion angles (φ, ψ) of the final DIPA model from *PROCHECK*. Glycine residues are shown in triangles and all other residues are squares. (*b*) Ramachandran plot for the main-chain torsion angles (φ, ψ) of the final DIPB model from *PROCHECK*. Glycine residues are shown in triangles and all other residues are squares.

side chains (Fig. 4). The density for residues 215–220 of DIPA is somewhat broken, although the connectivity is quite clear. Intermolecular contacts between residue CysB220, HisB146 and AspA97 of a symmetry-related monomer might give this portion of the main chain greater stability. Similar contacts are nonexistent between residues CysA220, HisA146 and a symmetry-related AspB97 residue. Instead, two ordered solvent molecules are within hydrogen-bonding distance of HisA146. The conformation of remaining active-site residues and the position of the covalently bound diisopropyl phosphoryl moieties are remarkably conserved in the two monomers. The orientations of the catalytic triad side-chain positions of residues Ser195 and Asp102 are consistent not only between the two monomers but also with those commonly seen in other serine proteases. The orientations of the HisA57 and HisB57 side chains are similar in the monomers, yet they are not found in the classical arrangement of the charge relay system. The imidazole ring exists in a *gauche+* conformation, DIPA $\chi 1 = 286°$ and DIPB $\chi 1 = 298°$, yet it is the *gauche−* conformation ($\chi 1 \simeq 60°$) which is normally observed in the active site of serine proteases (Janin, Wodak, Levitt & Maigret, 1978). It is likely that D undergoes a conformational change when bound to C3bB, facilitating the reorientation of these residues into the classical triad conformation.

The orientations of the DIP moieties in the individual monomers are relatively conserved. Each DIP moiety has one isopropoxy group extending down into the active site and one isopropoxy group protruding toward solvent. The phosphonyl O atom of each moiety is directed into the oxyanion hole, hydrogen bonded to the backbone amide N atoms of Gly193 and Ser195 residues as is common in serine proteases (Fig. 5).

3.2. *DIPA and DIPB comparison with native D*

The general architecture of the monomers of the native D structure and those inhibited by DFP are quite analogous, yet crucial differences can be seen in the arrangement of the catalytic triad and the active site of these enzymes (Fig. 5). The DIP:D monomers exhibit a closer similarity with the second monomer of native factor D structure, FADB (Table 2). SerB215

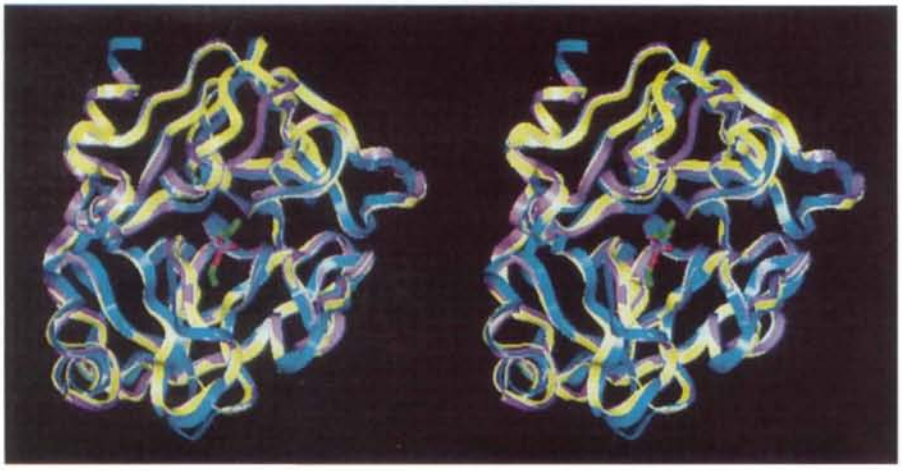

Fig. 2. Stereo ribbon diagram of the superposed structures of DIPB (yellow), FADB (magenta), and trypsin, of 4PTP (blue). All stereodiagrams were created utilizing the *Insight* II molecular modeling system.

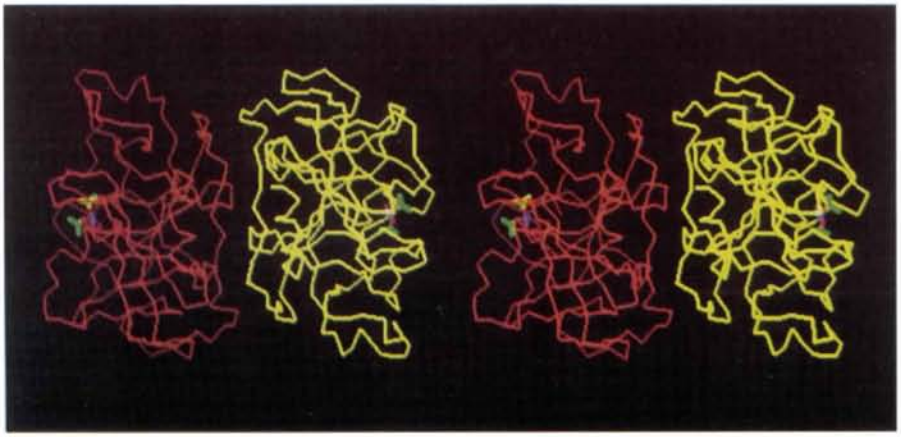

Fig. 3. Stereo Cα drawing of the DIPA (red) and DIPB (yellow) monomers. The DIP moieties are shown in the active sites, and colored by atom types.

of FADB blocks the imidazole ring from rotating to the 'in' conformation. In contrast, the FADA monomer displays a limited flexibility between residues A214 and A216, positioning AspA102 'out' of the classic triad orientation and HisA57 'in'. The imidazole rings of the respective catalytic histidines of the DIP:D monomers are both in the *gauche+* or 'out' orientation like FADB, yet the rings are rotated slightly out of plane with respect to each other. The SerA215 loop region of FADA is rotated down toward the bottom of the pocket, filling the primary specificity pocket in a manner like that of one of the isopropoxy moieties in the DFP derivatives. Although the Arg218:Asp189 salt bridge at the bottom of the pocket is intact in both the native and DIP:D monomers, the contacts are not identical. The Arg218 side chains of FADA and FADB penetrate deep into the pocket, involving both terminal N atoms of the guanidinium group in the salt bridge, while Arg218 of DIPA and DIPB utilizes only one N atom of the guanidinium group to bind to Asp189. The right-hand side of the active sites superpose well.

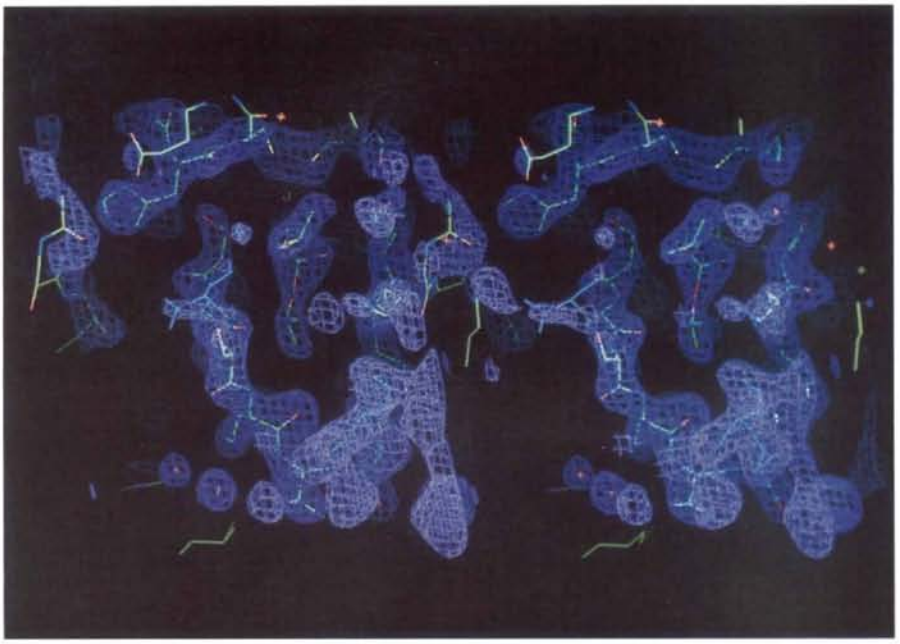

Fig. 4. Stereodiagram of the $(2F_o - F_c)$ electron-density map of the active site of DIPB.

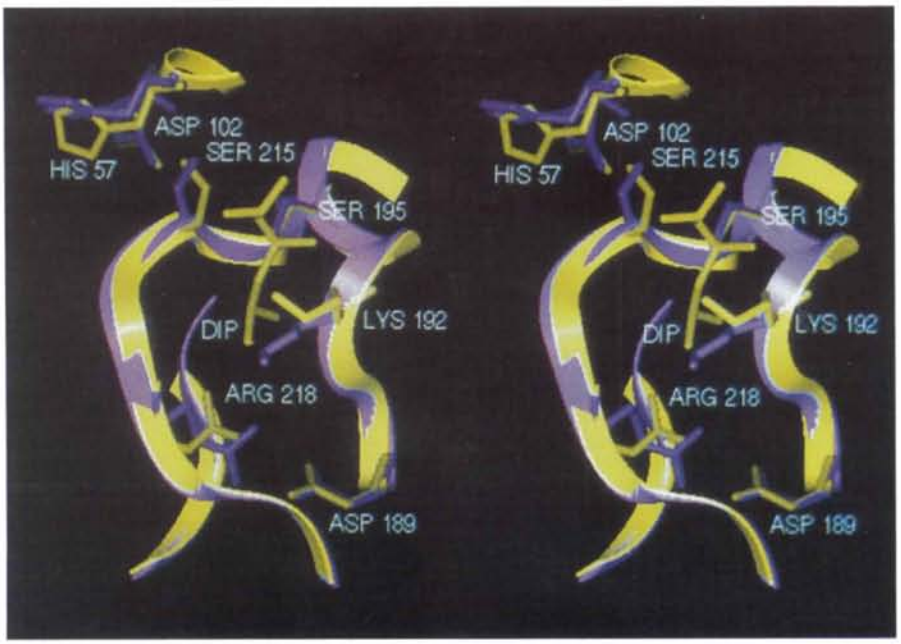

Fig. 5. Stereo ribbon diagram with selected residues shown as sticks of DIPB (yellow) and FADB (magenta).

Table 2. *R.m.s. deviation between Cα-atom positions*

Superposed structures	R.m.s. deviations
DIPA *versus* FADA	1.261
DIPB *versus* FADA	1.193
DIPA *versus* FADB	0.885
DIPB *versus* FADB	0.820

3.3. *DIP:D comparison with DIP:trypsin*

The superposition of DIPB with DIP-inhibited trypsin, 4PTP (Bernstein *et al.*, 1977), allows a detailed comparison between the active sites of the respectively inhibited enzymes and provides some insight into the different active-site specificity (Fig. 6). Again, the general folding patterns of the DIP:D and DIP:trypsin molecules are representative of the serine protease superfamily, with the principal variances observed in surface loops and the active-site regions, as would be expected. The 4PTP active site may be described as rather square in shape as viewed, while the P1 pockets of the DIP:D monomers appear more rounded. The respective catalytic Ser195 and Asp102 residues are almost identical, while the imidazole ring of histidine, His57, is 'in' (*gauche*−, $\chi 1 = 74°$) in 4PTP yet 'out' (*gauche*+) in DIPA and DIPB, as previously described. DIP-inhibited trypsin reveals only one isopropoxy group covalently bound to Ser195 in the active site, with the second isopropoxy group having been hydrolyzed (Chambers & Stroud, 1979). This single isopropoxy moiety fills the binding site of trypsin in the same manner as does the corresponding group of the DIP:D enzymes, extending down into the mouth of the DIPA and DIPB monomers. The right-hand side of the specificity pocket remains highly conserved in both amino-acid residue composition and architecturally among serine proteases, yet there is an interesting substitution at position 192 (Greer, 1990). Gln192 of trypsin (generally a Gln or Met in serine proteases) has been replaced by Lys192 in D. This change from a neutral to a charged amino-acid residue may be utilized for obtaining specificity for D. Other side chains which shape the active sites of these enzymes (Ser190 on the right, Tyr228 at the bottom and Val213 at the back center of the active sites) remain constant.

The left-hand side displays the major differences between these structures. There are key amino-acid substitutions at positions 215 and 218. Residue Trp215 of trypsin corresponds to Ser215 in D. The main chain of DIP:D monomers arches above the corresponding main-chain region of trypsin (as viewed in Fig. 6) and does not seem to move any side chain into the area voided by the substitution of a large amino-acid residue by a much smaller one. The lack of an Arg at position 218 in trypsin (Gly) as found in D precludes the formation of a salt bridge at the base of the pocket with Asp189. This amino-acid substitution provides a clear explanation for the lack of inhibition of many benzamidine-like trypsin inhibitors with respect to D.

3.4. *Discussion*

Attempts have been made to correlate the lack of a zymogen form of D with its low esterolytic activity toward thioester substrates and its high efficiency in activating the alternative complement pathway. It has been hypothesized that a conformational change of D is required to obtain the proteolytically active form of the enzyme, and must be induced by the natural substrate, C3b-complexed factor B. The imidazole ring of the active-site histidine of D must rotate about $\chi 1$ into the classical catalytic triad arrangement (*gauche*−) for enzymatic activity. Concurrently, Ser215 must shift to

Fig. 6. Stereo ribbon diagram with selected residues shown as sticks of DIPB (yellow) and DIP:trypsin (blue).

accommodate this rotation, in a similar manner to the native FADA monomer. Additionally, experiments have shown that mutations of Arg218 result in an almost complete loss of proteolytic activity of the enzyme, implicating a direct interaction between this amino-acid side chain and C3bB (Kim, Narayana & Volanakis, 1994). It is highly probable that the Arg218 side chain must break its intramolecular salt bridge and become exposed toward the solvent in order to form the active conformation of the enzyme. The exact nature of the interaction between Arg218 and bound factor B is unknown. However, the presence of the positively charged guanidinium group at the bottom of the P1 pocket influences both geometrical and electronic restraints which may be important when designing an enzyme inhibitor. These marked conformational shifts required for catalytic activity to be established are accommodated by the high degree of flexibility of the main-chain residues from 214 to 220 in the primary specificity pocket. Thus, two tracks must be considered in the design of novel small-molecule inhibitors of D. One is to focus on the native conformation of the enzyme; constructing a molecule which would bind tightly in the native active site. Locking the enzyme in the zymogen conformation would prohibit essential conformational changes from occurring, halting the alternative complement pathway activation. The second option is to design a molecule which would disrupt the intramolecular salt bridge of the enzyme, with a binding constant high enough to prevent access of the Arg233 of factor B to the primary specificity pocket. Both avenues are currently being explored in our search for a highly selective, tightly binding small-molecule inhibitor of D, capable of modulating the activation of the alternative complement pathway.

4. Addendum

As free R values, or $R_{\rm free}$ values (Brünger, 1992*b*), were not used in the initial stages of refinement, questions were raised concerning the validity of the 177.6° rotation angle between the two monomers, or whether the refinement should have been carried out imposing a 180.0° rotation angle and imposing non-crystallographic symmetry (NCS) restraints, refining only an appropriate weighting of NCS operators (Kleywegt & Brünger, 1996). Constraining the refinement requires that the NCS operators be held fixed throughout the refinement, forcing all copies of the molecule to be identical. If small variations between the molecules are allowed, the NCS operators are given weights which permit them to be refined. The refinement is then said to be restrained. $R_{\rm free}$ values can be used to test the appropriate degree to which the NCS operators should be allowed to vary, as was clearly shown by the work cited. *A posteriori* $R_{\rm free}$ values were then calculated as suggested, beginning with the final set of atomic coordinates and applying NCS restraints with varying weights. Surface loop regions were excluded from the equivalent groups. One round of simulated annealing and energy minimization was run, with a starting temperature of 4000 K. Runs with NCS weights of 0 (no restraints), 100, 300 and 3000 (effectively constrained) were conducted. The respective ΔR values ($R_{\rm free} - R$) for each run were 0.0802, 0.0820, 0.0938 and 0.0865. An NCS weight = 0 yielded the lowest overall R values ($R_{\rm free} = 0.2283$, $R = 0.1481$) compared with weight = 3000 ($R_{\rm free} = 0.2520$, $R = 0.1675$) and the lowest ΔR value, 0.0802 *versus* 0.0865. Combining this information with visual examination of the electron-density maps, we believe the monomers were best refined individually.*

This work was supported by BioCryst Pharmaceuticals, Inc. and the NIH (SBIR grant 1-R43-AR41095-01). The authors would like to thank Ms Debra Kellog for carefully proofreading the manuscript.

* Atomic coordinates and structure factors have been deposited with the Protein Data Bank, Brookhaven National Laboratory. Free copies may be obtained through The Managing Editor, International Union of Crystallography, 5 Abbey Square, Chester CH1 2HU, England (Reference GR0656).

References

Barnum, S. R., Niemann, M. A., Kearney, J. F. & Volanakis, J. E. (1984). *J. Immunol. Methods*, **67**, 303–309.

Bernstein, F. C., Koetzle, T. F., Williams, G. J. B., Meyer, E. F., Brice, M. D., Rodgers, J. R., Kennard, O., Shimanouchi, T. & Tasumi, M. (1977). *J. Mol. Biol.* **112**, 535–542.

Brünger, A. T. (1990). *Acta Cryst.* A**46**, 46–57.

Brünger, A. T. (1992*a*). *X-PLOR. A System for X-ray Crystallography and NMR.* Version 3.1. New Haven and London: Yale University Press.

Brünger, A. T. (1992*b*). *Nature (London)*, **355**, 472–475.

Bugg, C. E., Carson, W. M. & Montgomery, J. A. (1993). *Sci. Am.* **269**(6), 92–98.

Chambers, J. L. & Stroud, R. M. (1979). *Acta Cryst.* B**35**, 1861–1874.

Cryer, H. G., Richardson, J. D., Longmire-Cook, S. & Brown, C. M. (1989). *Arch. Surg.* **124**, 1378–1385.

Fearon, D. T., Austen, K. F. & Ruddy, S. (1974). *J. Exp. Med.* **139**, 355–366.

Greer, J. (1990). *Proteins*, **7**, 317–334.

Hansson, G. K., Jonasson, L., Seifert, P. S. & Stemme, S. (1989). *Atherosclerosis*, **9**, 567–578.

Howard, A. J., Gilliland, G. L., Finzel, B. C., Poulos, T. L., Ohelendorf, D. H. & Salemme, F. R. (1987). *J. Appl. Cryst.* **20**, 383–387.

Janin, J., Wodak, S., Levitt, M. & Maigret, B. (1978). *J. Mol. Biol.* **125**, 357–386.

Jones, T. A. (1978). *J. Appl. Cryst.* **11**, 268–272.

Kam, C.-M., McRae, B. J., Harper, J. W., Niemann, M. A., Volanakis, J. E. & Powers, J. C. (1987). *J. Biol. Chem.* **262**, 3444–3451.

Kam, C.-M., Oglesby, T. J., Pangburn, M. K., Volanakis, J. E. & Powers, J. C. (1992). *J. Immunol.* **149**, 163–168.

Kim, S., Narayana, S. V. L. & Volanakis, J. E. (1994). *Biochemistry*, **33**, 14393–14399.

Kleywegt, G. J. & Brünger, A. T. (1996). *Structure*, **4**(8), 897–904.

Laskowski, R. A., MacArthur, M. W., Moss, D. S. & Thornton, J. M. (1993). *J. Appl. Cryst.* **26**, 283–291.

Lesavre, P. H., Hugli, T. E., Esser, A. F. & Muller-Eberhard, H. J. (1979). *J. Immunol.* **123**, 529–534.

Lesavre, P. H. & Muller-Eberhard, H. J. (1978). *J. Exp. Med.* **148**, 1498–1509.

Narayana, S. V. L., Carson, M., El-Kabbani, O., Kilpatrick, J. M., Moore, D., Chen, X., Bugg, C. E., Volanakis, J. E. & DeLucas, L. J. (1994). *J. Mol. Biol.* **235**, 695–708.

Niemann, M. A., Brown, A. S., Bennett, J. C. & Volanakis, J. E. (1984). *Biochemistry*, **23**, 2482–2486.

Thaller, C., Weaver, L. H., Eichele, E., Wilson, E., Karlsson, R. & Jansonius, J. N. (1981). *J. Mol. Biol.* **147**, 465–469.

Volanakis, J. E., Barnum, S. R. & Kilpatrick, J. M. (1993). *Methods Enzymol.* **223**, 82–97.

Volanakis, J. E. & Macon, K. J. (1987). *Anal. Biochem.* **163**, 242–246.

Yasuda, M., Takeuchi, K., Hiruma, M., Iida, H., Tahara, A., Itagane, H., Toda, I., Akioka, K., Teragaki, M., Oku, H., Kanayama, Y., Takeda, T., Kolb, W. P. & Tamerius, J. D. (1990). *Circulation*, **81**(1), 156–163.